Stimulated degenerate four-wave mixing in Si nanocrystal waveguides

2016 J. Opt. 18 075801

(http://iopscience.iop.org/2040-8986/18/7/075801)

IOP Publishing Journal of Optics
J. Opt. 18 (2016) 075801 (8pp) doi:10.1088/2040-8978/18/7/075801

Stimulated degenerate four-wave mixing in Si nanocrystal waveguides

Santanu Manna[1], Martino Bernard[2], Stefano Biasi[1], Fernando Ramiro Manzano[1], Mattia Mancinelli[1], Mher Ghulinyan[2], George Pucker[2] and Lorenzo Pavesi[1]

[1] Laboratorio di Nanoscienze, Dipartimento di Fisica, Universita di Trento, Via Sommarive 14, 38123 Povo (Trento), Italy
[2] Centre for Materials and Microsystems, Fondazione Bruno Kessler, via Sommarive 18, 38123 Povo (Trento), Italy

E-mail: santanu.manna@unitn.it

Received 3 March 2016, revised 30 April 2016
Accepted for publication 9 May 2016
Published 14 June 2016

Abstract

Parametric frequency conversion via four-wave mixing (FWM) in silicon nanocrystal (Si NC) waveguides is observed at 1550 nm. To investigate the role of Si NC, different types of waveguides containing Si NC in a SiO_2 matrix were fabricated. Owing to the increase of the dipole oscillator strength mediated by the quantum confinement effect, the non-linear refractive index (n_2) of Si NCs is found to be more than one order of magnitude larger than the one of bulk Si. Coupled differential equations for the degenerate FWM process taking into account the role of Si NC were numerically solved to model the experimental data. The modeling yields an effective n_2 for Si NCs in SiO_2 waveguides which is similar to the one of Si waveguides. We also measured a large signal to idler conversion bandwidth of ~22 nm. The large non-linear refractive index is joined with a large two photon absorption coefficient which makes the use of Si NC in non-linear optical devices mostly suitable for mid-infrared applications.

Keywords: four wave mixing, Si nanocrystal, waveguide, silicon photonics

(Some figures may appear in colour only in the online journal)

1. Introduction

Motivated by the request of an interconnect technology with large bandwidth and with low power consumption, silicon photonics is achieving the on-chip convergence between electronics and photonics [1]. In this way, a cost-effective mass production manufacturing technology is available for photonic devices. Generation and manipulation of light is feasible in ultra-compact multi-functional chips owing to the strong third order nonlinearities of silicon [2–7]. In addition, silicon composite materials such as silicon nitride [8, 9] or silicon nanocrystals (Si NC) in silica matrix [10, 11] are emerging as alternative nonlinear materials due to either a negligible two photon absorption or to a high third order optical nonlinearity, respectively [12–18]. Generally, a high linear refractive index in the active material yields strong nonlinearity. Here, Si NCs are appealing since they have both a strong nonlinearity and a low linear refractive index. Their high third order nonlinearity is explained by the enhancement of the oscillator strength due to quantum confinement of carriers and by the large dielectric mismatch between the Si core and the embedding silica matrix. Since Si NCs are fabricated by using standard CMOS processing tools, they represent a viable route to integrate a nonlinear active material in CMOS technology [10, 11].

In recent years, the third order nonlinearity of Si NCs and other material systems (like 2D graphene, topological insulators etc) has been studied by many groups, mostly by z-scan techniques of thin films [14–17, 19, 20]. Applications of the Si NC nonlinearities in nonlinear optical devices appeared as well, e.g., ultra-fast all optical switching in horizontal Si NC slot waveguide based ring resonators [13], new frequency generation through four wave mixing (FWM) in horizontal slot waveguides [18, 21], and spatial multimode interference profile mapping using two photon absorption (TPA) [22]. It is noteworthy that Si NCs could act as scattering centers for

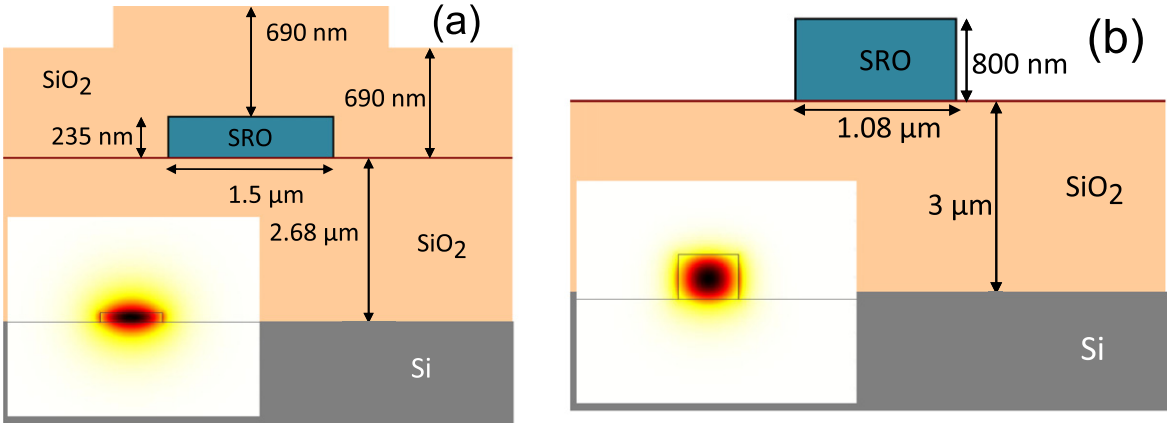

Figure 1. (a) Cross section of a Si NC channel waveguide with dimension of 235 nm × 1500 nm; inset shows the TE fundamental mode profile, and (b) cross section of a Si NC stripe waveguide with dimension of 800 nm × 1080 nm; inset shows the TE fundamental mode profile. SRO refers to the silicon rich silicon oxide region where the Si NCs formed.

light propagation in a waveguide, resulting in increased propagation losses. The propagation losses measured at 1550 nm are 3–4 dB cm^{-1} [22].

Since in many of the previous works, Si NCs were placed in a slot waveguide configuration [13, 18, 21, 23], there is the need of an assessment of the Si NC nonlinearity in a Si NC waveguide. This is the aim of our work. By studying the stimulated degenerate four wave mixing (FWM) we derive an estimate of different nonlinear parameters: the nonlinear refractive index (n_2), the TPA coefficient (β_{TPA}), the excited carrier lifetime (τ), and the excited carrier cross section (σ_{ECA}). To extract these parameters, we model the FWM process in a Si NC composite waveguide by nonlinear propagation equations.

2. Sample details

The plasma enhanced chemical vapor deposition (PECVD) technique was used to deposit the silicon rich silicon oxide (SRO) layer on top of a 4 μm thick thermal silica coated Si wafer. The SRO layer is deposited from a mixture of silane (SiH_4, 94 sccm) and nitrous oxide (N_2O, 945 sccm) gases. Post deposition annealing for 1.5 h at 1150 °C in an N_2 atmosphere leads to a phase separation of Si and SiO_2 and, hence, to the formation of Si NCs in a silica host. Elipsometric measurements yield a material's refractive index of 1.953 at 1550 nm. Waveguides of two different geometries were defined by optical lithography and reactive ion etching: (1) 235 nm × 1500 nm channel waveguide, cladded with a PECVD SiO_2, and, thus, totally buried within silica (shown in figure 1(a)), and (2) 800 nm × 1080 nm stripe waveguide laying on top of the silica lower cladding (shown in figure 1(b)). In the following, we refer to these waveguides as WG(channel) and WG(stripe), respectively. Linear propagation losses of the fundamental transverse electric (TE) polarized mode at 1550 nm were measured and accounted for 3.4 ± 0.2 dB cm^{-1} and 3.0 ± 0.5 dB cm^{-1} for the WG(channel) and WG(stripe), respectively. Insertion losses and damage threshold were 10 dB and 100 GW cm^{-2} for both waveguides.

3. Modeling

Finite element simulations (based on the COMSOL suite) were employed to obtain the modal behavior of the waveguides. Insets of figures 1(a) and (b) show the modal profile for the fundamental TE mode.

To include the effects of the quantum confinement of the Si NC electronic states in the simulation of the FWM process, we consider the volume fraction of Si in the composite material, which makes the core of the waveguides. Indeed, the FWM process occurs mainly due to the Si NC polarization while the silica matrix is assumed to be passive in this process. Therefore, the refractive index of the materials which generate the nonlinear interaction is the one of the Si NC, i.e. the silicon one. On the other hand, the light-waves propagation along the waveguide is ruled by the effective index (n_{eff}) of the optical mode which is caused by the whole core material. In the literature, FWM simulations of the Si NC system were performed either by assuming the effective medium approach without imposing quantum confinement effects [24, 25] or by studying the dielectric function of one isolated Si NC through the atomistic pseudo-potential calculation of n_2 and the nonlinear component of the absorption coefficient (β_{TPA}) [26]. Here, we consider both effects by using a phenomenological approach.

3.1. Two photon absorption coefficient

From the photoluminescence spectra of the Si NC material [22], we can estimate that the average Si NC band gap is ~1.51 eV. This value is less than twice the 1550 nm photon energy, i.e. TPA is possible. To link the measured TPA coefficient with the one characteristic of the isolated nanocrystal, a weighted average on the composite (Si NC embedded in a silica matrix) nature of the waveguide has to be considered. It was calculated in [25] that the proper way to

take this effect into account is to use $\xi\beta_{\mathrm{TPA}}$ for the effective TPA coefficient of the waveguide, where

$$\xi = \frac{[(3f-1)\varepsilon_{\mathrm{eff}} + \varepsilon_{\mathrm{Si}}]^2}{f(u^2 + 8\varepsilon_{\mathrm{Si}}\varepsilon_{ox})} \tag{1}$$

is the third order susceptibility attenuation factor [25]. In equation (1), $\varepsilon_{\mathrm{eff}}$ is the effective dielectric function of the Si NCs/SiO_2 composite. $\varepsilon_{\mathrm{eff}}$ can be computed by using the effective medium theory [27, 28] by

$$\varepsilon_{\mathrm{eff}} = \frac{u + \sqrt{u^2 + 8\varepsilon_{\mathrm{Si}}\varepsilon_{ox}}}{4} \tag{2}$$

where $\varepsilon_{\mathrm{Si}}$ is the dielectric function of silicon, ε_{ox} that of silica, $u = (3f-1)\varepsilon_{\mathrm{Si}} + (2-3f)\varepsilon_{ox}$ and f is the volume fraction of Si in the composite. For the waveguides under investigation, the Si volume fractions are 27% and 28.4% for WG(channel) and WG(stripe), respectively. With these parameters, we obtain for ξ 0.036 and 0.041 for WG(channel) and WG(stripe), respectively. This suggests that the TPA coefficient of a single NC is more than one order of magnitude larger than that of the whole Si NCs/SiO_2 composite. TPA coefficients were evaluated using the power dependence of the transmittance [22]. It was found $\xi\beta_{\mathrm{TPA}} \sim 0.4$ m/GW, which is more than one order of magnitude larger than the bulk value. This value agrees with the one found by z-scan measurements [12].

3.2. FWM propagation equation

For a stimulated degenerate four wave mixing process, two degenerate pump photons mix with a signal photon to generate the idler photon. For an efficient frequency generation, the energy and the momentum should be conserved. Energy conservation can be written in terms of the pump λ_p, the signal λ_s and the idler λ_c photon wavelengths as $2/\lambda_p = 1/\lambda_s + 1/\lambda_c$. Momentum conservation implies phase matching of the three interacting waves. This is determined by the energies of the three waves and by the dispersion nature of the refractive index of the waveguide. We can define the pump power dependent total phase difference (κ) as the phase mismatch between the three waves by:

$$\begin{aligned}\kappa &= \Delta\beta + 2\gamma_p P_p = \beta_s + \beta_c - 2\beta_p + 2\gamma_p P_p \\ &= (\tilde{n}_s\, h\nu_s + \tilde{n}_c\, h\nu_c - 2\tilde{n}_p\, h\nu_p)/c + 2\gamma_p P_p\end{aligned} \tag{3}$$

where $\tilde{n}_i$ is the effective mode index of the wave with the frequency ν_i, the subscripts $i = p$, s or c refer to the pump, the signal and the idler waves, respectively, h is the Planck constant, P_p the pump wave power, $\gamma_i = n_2\omega_i/(cA_{\mathrm{eff}})$ is the non-linearity parameter at angular frequency ω_i and A_{eff} the effective mode area [29] which for the TE polarized mode at 1550 nm is 1.03 and 1.01 μm^2 for the WG(channel) and WG(stripe), respectively

In the waveguide, the propagation of the three waves is described by three coupled nonlinear Schrodinger equations. Considering the linear propagation loss, the TPA and the excited carrier absorption (ECA), and using the quasi-continuous wave approximation, the coupled equations for the degenerate FWM process can be written as [30]

$$\begin{aligned}\frac{dA_p}{dz} &= -\frac{1}{2}(\alpha_p + \alpha_{\mathrm{TPA}p} + \alpha_{\mathrm{ECA}p})A_p \\ &\quad + j\gamma_p\xi[\psi_1\,|A_p|^2 + 2\psi_2\,|A_s|^2 + 2\psi_2\,|A_c|^2] \\ &\quad + 2j\gamma_p\xi\psi_1 A_p{}^* A_s A_c \exp(j\Delta\beta z)\end{aligned} \tag{4a}$$

$$\begin{aligned}\frac{dA_s}{dz} &= -\frac{1}{2}(\alpha_s + \alpha_{\mathrm{TPA}s} + \alpha_{\mathrm{ECA}s})A_s \\ &\quad + j\gamma_s\xi[2\psi_2\,|A_p|^2 + \psi_1\,|A_s|^2 + 2\psi_2\,|A_c|^2] \\ &\quad + j\gamma_s\xi\psi_1 A_c{}^* A_p A_p \exp(-j\Delta\beta z)\end{aligned} \tag{4b}$$

$$\begin{aligned}\frac{dA_c}{dz} &= -\frac{1}{2}(\alpha_c + \alpha_{\mathrm{TPA}c} + \alpha_{\mathrm{ECA}c})A_c \\ &\quad + j\gamma_c\xi[2\psi_2\,|A_p|^2 + 2\psi_2\,|A_s|^2 + \psi_1\,|A_c|^2] \\ &\quad + j\gamma_c\xi\psi_1 A_s{}^* A_p A_p \exp(-j\Delta\beta z)\end{aligned} \tag{4c}$$

where A_i is the electric field amplitude of the propagating wave, $\psi_1 = (8+7\rho)/45$ is the factor which considers self phase modulation processes, $\psi_2 = (29+16\rho)/45$ is the factor which considers cross phase modulation processes and ρ is the nonlinear anisotropy factor ($\rho \approx 1.27$) [24, 25]. The TPA and the ECA processes are described in equation (4*a*) by

$$\alpha_{\mathrm{TPA}i} = \frac{(\xi\beta_{\mathrm{TPA}})}{A_{\mathrm{eff}}}\left(\psi_1\,|A_i|^2 + 2\psi_2\sum_{m\neq i}|A_m|^2\right) \tag{5}$$

$$\begin{aligned}\alpha_{\mathrm{ECA}i} = \frac{(\zeta\sigma_{\mathrm{ECA}i})(\xi\beta_{\mathrm{TPA}})\tau}{2hc{A_{\mathrm{eff}}}^2}\Bigg[&\psi_1{}^2\sum_m \lambda_m\,|A_m|^4 \\ &+ 4\psi_2{}^2\sum_{m\neq n}\frac{\lambda_m\lambda_n\,|A_m|^2|A_n|^2}{\lambda_m+\lambda_n}\Bigg]\end{aligned} \tag{6}$$

where the summation runs on the different waves (indexed by m). Here, ζ is the linear susceptibility attenuation factor defined as

$$\zeta = \left(\frac{\varepsilon_{\mathrm{Si}}}{\varepsilon_{\mathrm{eff}}}\right)^{1/2}\frac{(3f-1)\varepsilon_{\mathrm{eff}} + \varepsilon_{ox}}{\sqrt{u^2 + 8\varepsilon_{\mathrm{Si}}\varepsilon_{ox}}}. \tag{7}$$

Calculated values of ζ for WG(channel) and WG(stripe) are 0.181 and 0.196, respectively. It is worth to mention that if β_{TPA}, n_2 and σ_{ECA} are for a single NC, $\xi\beta_{\mathrm{TPA}}$, ξn_2 and $\zeta\sigma_{\mathrm{ECA}}$ are the effective values for the SiNC/SiO_2 waveguide as a whole. The attenuation factors ξ, ζ reduce the nonlinear parameters of the whole composite compared to those of the individual nanocrystal.

3.3. Group index and group velocity dispersion

By modal analysis of the waveguides with the values of the wavelength dependent refractive index measured by ellipsometry, we calculated the group index and the group velocity dispersion (GVD). Figure 2(a) shows that the group index is smaller for WG(stripe) than for WG(channel) because of a better mode confinement in WG(stripe). Figure 2(b) shows the GVD parameter $D = -\frac{2\pi c}{\lambda^2}\beta_2$ (where $\beta_2 = \frac{\lambda^3}{2\pi c^2}\frac{d^2 n_{\mathrm{eff}}}{d\lambda^2}$). WG(channel) shows a normal dispersion around 1550 nm, whereas WG(stripe) shows a region of anomalous dispersion at 1550 nm. This results from a fine adjustment of the

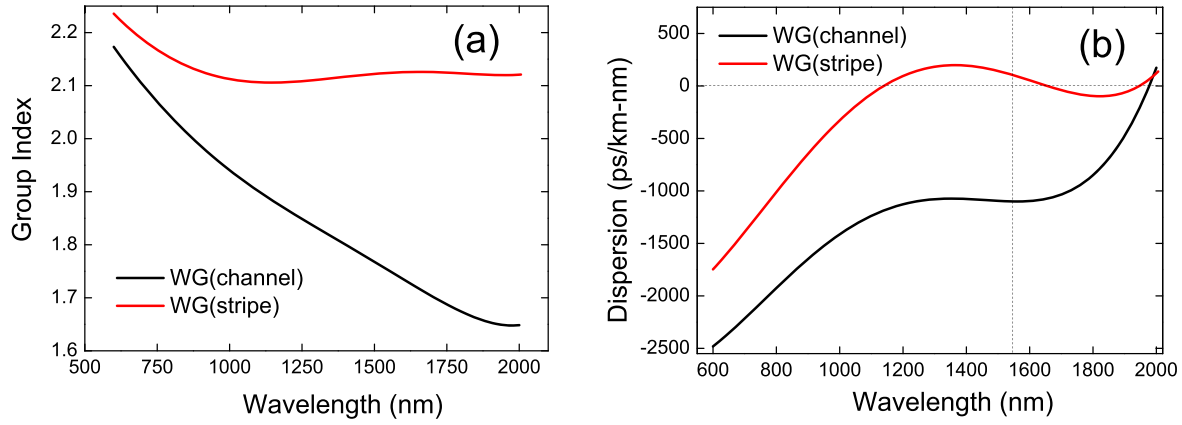

Figure 2. (a) Calculated group index and (b) group velocity dispersion D of the TE mode for both of the waveguides used in this study.

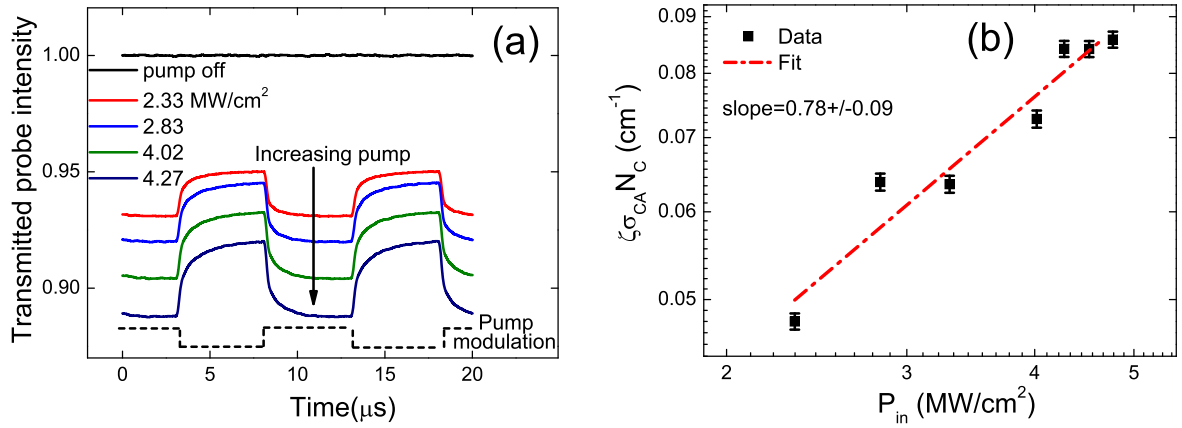

Figure 3. (a) Time dependence of the probe signal intensity at 1545 nm for different pump signal powers. The pump signal modulation is shown as the dotted line at the bottom of the graph. Measurements refer to WG(stripe). (b) Excited carrier absorption cross section ($\zeta\sigma_{\mathrm{ECA}}$) times the excited carrier density (N_C) at 1545 nm as a function of the pump signal power density for WG(stripe). The slope of the linear fit is 0.78 ± 0.09.

waveguide dimension and due to the absence of an upper cladding. Due to the improper phase matching for WG(channel), a lower performance is expected in idler generation compared to WG(stripe) waveguide.

4. Excited carrier lifetime and absorption cross section measurements

Due to the important role of excited carriers, we performed a detailed measurement of the excited carrier losses. These were measured by using a pump-probe technique [31]. Two tunable lasers provide the pump and probe signals. A semiconductor optical amplifier (SOA) was used to amplify the pump signal which was then fed into an electro-optic modulator with ns time resolution to switch it on and off. The modulated pump signal was further amplified by an Erbium doped fiber amplifier (EDFA) and filtered by a tunable narrow bandpass filter. The pump signal was thereafter combined with the probe signal using a 3-dB coupler. Both signals were then coupled into the Si NC waveguide by using a tapered lens fiber. Polarizations of the pump and of the probe signals were fixed by a polarization controller. The transmitted signal was collected by a tapered lens fiber followed by a filtering stage to eliminate the residual pump. The probe signal was then analysed by an optical spectrum analyser (OSA). The pump wavelength was fixed to 1550 nm, which is the one used for the FWM measurements, while the probe wavelength was 1545 nm. Figure 3(a) shows the time dependence of the probe signal transmission for different pump signal powers. When the pump is ON, excited carriers are generated in the waveguide due to TPA. Consequently the transmitted probe signal intensity decreases. Note that the different transmitted signals are offset by a thermal contribution which comes from waveguide heating due to carrier relaxation. When the pump is turned OFF, excited carriers recombine and the transmitted probe signal intensity recovers. Therefore, the excited carrier lifetime can be extracted from the recovery of the probe signal after switching OFF the pump.

By measuring the ratio SE between the transmitted probe signal intensity when the pump is ON (I_{p-p}) and the transmitted probe signal intensity when the pump is OFF (I_{probe}), i.e. $SE = I_{p-p}/I_{\mathrm{probe}}$, the ECA loss coefficient (α_{ECA}) as a

function of pump signal power can be extracted as [31]

$$\alpha_{\mathrm{ECA}} = \zeta\sigma_{\mathrm{ECA}} N_c = -\frac{\ln(SE)}{\Gamma L} \tag{8}$$

where Γ is the confinement factor of the optical mode. In our case, $\Gamma = 0.343$ for WG(channel) and $\Gamma = 0.858$ for WG(stripe) at 1550 nm for the TE polarized fundamental mode.

The ECA loss coefficient α_{ECA} as a function of the pump signal intensity is plotted in a log-log graph in figure 3(b). Data can be fitted by a straight line of slope 0.78 ± 0.09, suggesting the presence of Auger dominated excited carrier recombination processes [31]. For the highest power density value used (4.77MW cm^{-2}), $\zeta\sigma_{\mathrm{ECA}} N_c = 0.086$ cm^{-1} = 0.37 dB cm. Considering one carrier per Si NC, the effective carrier absorption cross section $\zeta\sigma_{\mathrm{ECA}}$ of WG(stripe) results to be $\sim 2.5 \times 10^{-20}$ cm^2 when the density of NCs is 3.5×10^{18} cm^{-3}. This $\zeta\sigma_{\mathrm{ECA}}$ value is more than two orders of magnitude lower than what found in bulk Si [31]. However, the $\alpha_{\mathrm{ECA}i}$ terms, which enter in equation (4*a*) and which are responsible for the ECA loss in nonlinear experiments, are approximately one order of magnitude larger than the bulk Si value because of the other factors which enter in equation (6). For WG(channel), $\zeta\sigma_{\mathrm{ECA}} = 2.45 \times 10^{-19}$ cm^2 at a power density of 5.73MW cm^{-2}, being close to the one reported earlier [31]. The carrier lifetime extracted from the raise of the transmitted probe signal is $3 \pm 1\mu$s and $31 \pm 1\ \mu$s for WG(stripe) and WG(channel), respectively. It is noteworthy that the time scale of the PL decay at 800 nm and of the ECA at 1550 nm are similar [31]. In addition, the scaling of the waveguide dimensions causes the carrier lifetime shortening for WG(stripe). As reported in [32], the width to height ratio (W/H) of ridge waveguides influences the carrier lifetime through the change in the transit time for the excited carriers to diffuse to the waveguide surfaces where recombination mainly occurs. The smaller is the W/H ratio, the shorter is the transit time and the shorter is the excited carrier lifetime. In our case, W/H ratios are 1.4 and 6.4, for WG(stripe) and WG(channel), respectively, which explains the almost one order of magnitude longer lifetime for WG(channel) compared to WG(stripe).

5. Stimulated degenerate FWM measurements

Stimulated degenerate FWM measurements have been performed on 5 mm long waveguides by fixing the pump wavelength near 1550 nm and by varying the signal wavelength in a range from 1550 to 1575 nm. Consequently, the idler signal was measured at shorter wavelengths than the pump wavelength. The measurement setup consisted in two tunable lasers that provide the pump and signal beams. Both the pump and signal beams were amplified by EDFAs, polarization controlled and filtered by a band pass filter to remove the amplified spontaneous emission (ASE) contribution of the EDFA. The signal intensity was further tuned by a variable optical attenuator (VOA). After a coupler which overlaps the pump and the signal beams in a single fiber, 10% of the input signal is sent to an OSA for monitoring. A tapered lens fiber was used to couple the pump and signal waves into the Si-NC waveguide. An isolator was used before the waveguide to ensure that no signal generation occurs in the fibers due to the back reflection from the waveguide facet. The output transmission from the waveguide was collected by a tapered lens fiber and analyzed by an optical spectrum analyzer (OSA) or a photodiode (PD).

An example of a characteristic FWM spectrum for WG(channel) is shown in figure 4(a). Since both the input waves have similar intensities, two idler waves are generated at frequencies $\nu_{c,1} = 2\nu_p - \nu_s$ and $\nu_{c,2} = 2\nu_s - \nu_p$. We have noticed that when the pump and signal intensities decrease, the idler wave which peaks at $\nu_{c,2}$ vanishes (figure 4(b)). This fact is explained by making the following considerations: on one side, the idler wave at $\nu_{c,1}$ is associated with two pump photons at ν_p and one signal photon at ν_s, therefore, the idler wave intensity should vary quadratically with the pump wave intensity and linearly with the signal wave intensity. On the other hand, the idler wave intensity at $\nu_{c,2}$ should vary linearly with pump wave intensity and quadratically with the signal wave intensity. These trends have been indeed observed which allows to assign the origin of the two idler waves. Similar FWM spectrum have been observed for WG(stripe). The symmetric variation of the idler generation could be observed from WG(stripe) in figure 4(c).

Figure 5(a) presents the idler ($\nu_{c,1}$) to signal intensity ratio as a function of the pump power in the WG(channel) waveguide. For low pump wave power, idler to signal ratio is quadratic as it is expected. By increasing the pump power, this ratio departs from the quadratic dependence and tends to saturate due to the contribution of nonlinear losses such as TPA and TPA assisted ECA. The longer is the excited carrier lifetime, the lower are the pump power values at which conversion efficiency saturation occurs (figure 5, compare the two simulation curves). By estimating the ratio via equation (4*a*) and fitting the parameters to the experimental data, we have extracted a value of $n_2 = 1.2 \times 10^{-16}$ m^2/W for WG(channel). Table 1 reports the values of the different fitting parameters. The extracted n_2 value is more than one order of magnitude larger than the bulk Si value [30]. On the other hand, fitting the data with simulation for WG(stripe) yields $n_2 = 0.9 \times 10^{-16}$ m^2/W. The values extracted from the FWM modeling in our experiments are consistent with previous reports. In fact, earlier works by Spano *et al* [12] using Z-scan measurements reported that Si NC/SiO_2 films with a Si excess of 27% (our waveguides have a Si excess of 28.4%) have $n_2 \sim 4 \times 10^{-17}$ m^2/W; Martinez *et al* [13] quoted $n_2 \sim 4 \times 10^{-17}$ m^2/W for PECVD grown Si NCs/SiO_2 with 8% Si excess and $n_2 \sim 2 \times 10^{-16}$ m^2/W for LPCVD (low pressure CVD) grown Si NCs/SiO_2; Trita *et al* [21] reported $n_2 \sim 3.7 \times 10^{-17}$ m^2/W for the TM mode in an horizontal slot waveguide; Ito *et al* [17] showed an increase in the n_2 values from $\sim 10^{-17}$ to $\sim 10^{-16}$ m^2/W depending on the Si excess; theoretical simulation in [26] using pseudo-potential approach, which considered quantized electronic states of Si NCs, obtained estimate of n_2 consistent with our data. Note that the large n_2 value characteristic of Si NC is reduced when

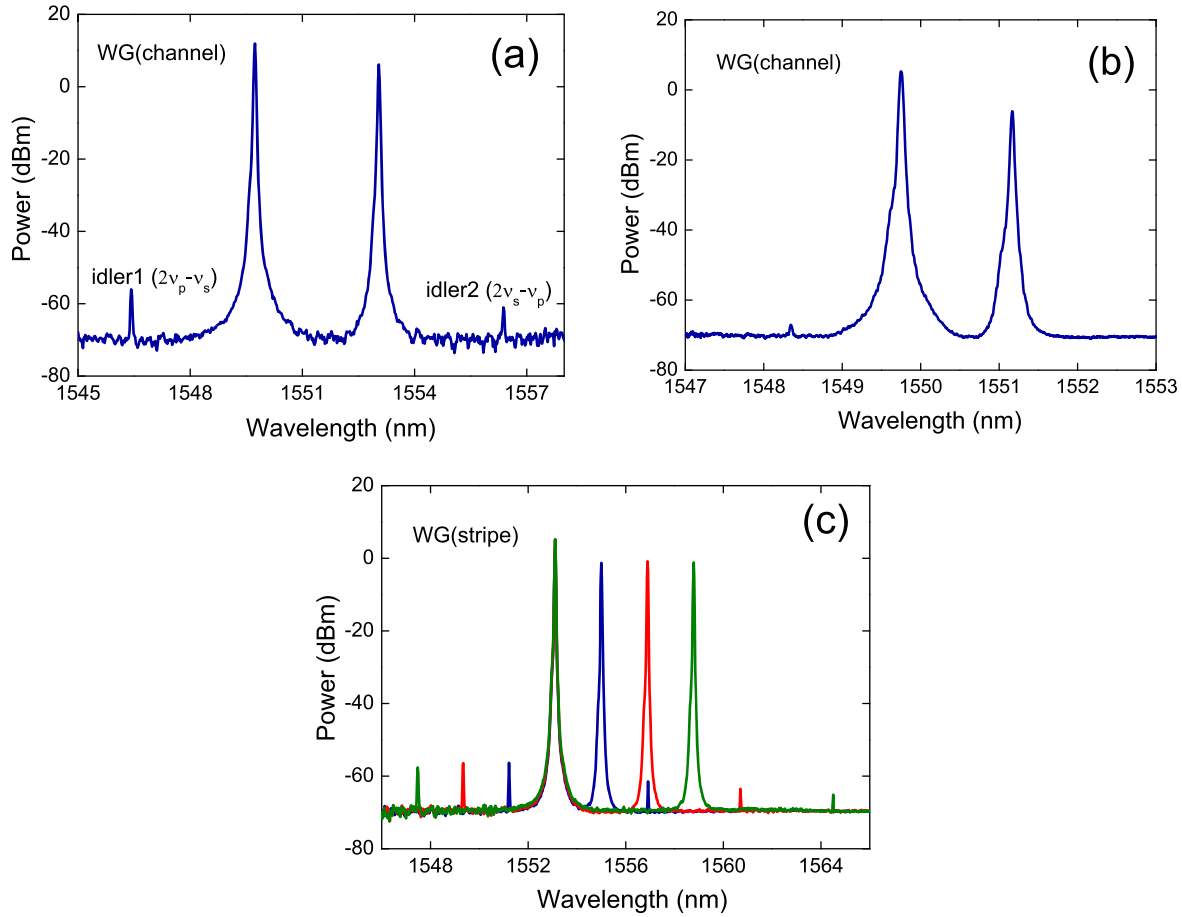

Figure 4. (a) Typical FWM spectrum for the WG(channel) waveguide ($P_{\text{pump}} = 15.5$ mW; $P_{\text{signal}} = 4$ mW) (b) same for the WG(channel) waveguide ($P_{\text{pump}} = 12$ mW; $P_{\text{signal}} = 0.8$ mW). (c) Same for the WG(stripe) waveguide ($P_{\text{pump}} = 31.8$ mW; $P_{\text{signal}} = 5.9$ mW).

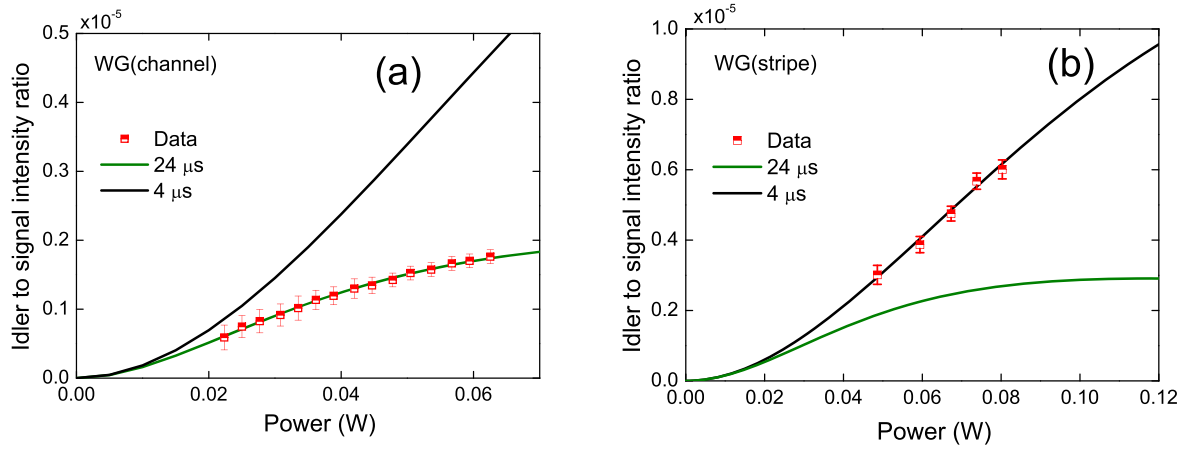

Figure 5. Idler to signal intensity ratio as a function of the pump power for (a) WG(channel) and (b) WG(stripe) waveguides. The solid lines correspond to simulation while the squares denote the experimental data. Two simulations are shown where the best fit parameters (table 1) are used and, only, the excited carrier lifetimes are varied.

the effect of the matrix is considered as in the waveguide. In this case, the propagating optical wave interacts with the overall composite core of the waveguide and the effective ξn_2 has to be considered. Consequently, the measured value is more than an order of magnitude reduced and approaches to the one of Si waveguides. This shows that when dealing with Si NC not only the size is relevant but also their concentrations. In fact, by increasing the concentration of Si NC in the waveguide ξ decreases and the effective ξn_2 increases the waveguide nonlinearities.

In actual waveguide, mode confinement can be also tailored to increase the waveguide nonlinearity. This is quantified by the waveguide nonlinearity parameter γ, which counts to 17,000 $\pm$ 2,000 and 15,000 $\pm$ 3,000 W^{-1} km^{-1} for

Table 1. Numerical values of the parameters used for the fitting in figure 5.

	Design	WG(channel)	WG(stripe)
	Signal power (mW)	4.1	0.8
	waveguide length (mm)	5.0	5.0
	α (dB cm^{-1})	3.4 ± 0.2	3.0 ±0.2
	τ (μs)	24 ± 4	4 ± 3
Individual NC	n_2 (m^2/W)	1.2 ± 0.2 ×10^{-16}	0.9 ± 0.2 ×10^{-16}
	β (m/W)	6 ± 2 ×10^{-9}	8 ± 2 ×10^{-9}
	σ_{ECA} (cm^2)	5.5 ± 3 ×10^{-19}	1.8 ± 0.5 ×10^{-19}
Composite	ξn_2 (m^2/W)	4.4 ± 0.6 ×10^{-18}	3.8 ± 0.7 ×10^{-18}
	$\xi\beta$ (m/W)	2.0 ± 0.8 ×10^{-10}	3 ± 1 ×10^{-10}
	$\zeta\sigma_{ECA}$ (cm^2)	1.0 ± 0.5 ×10^{-19}	3.5 ± 1 ×10^{-20}

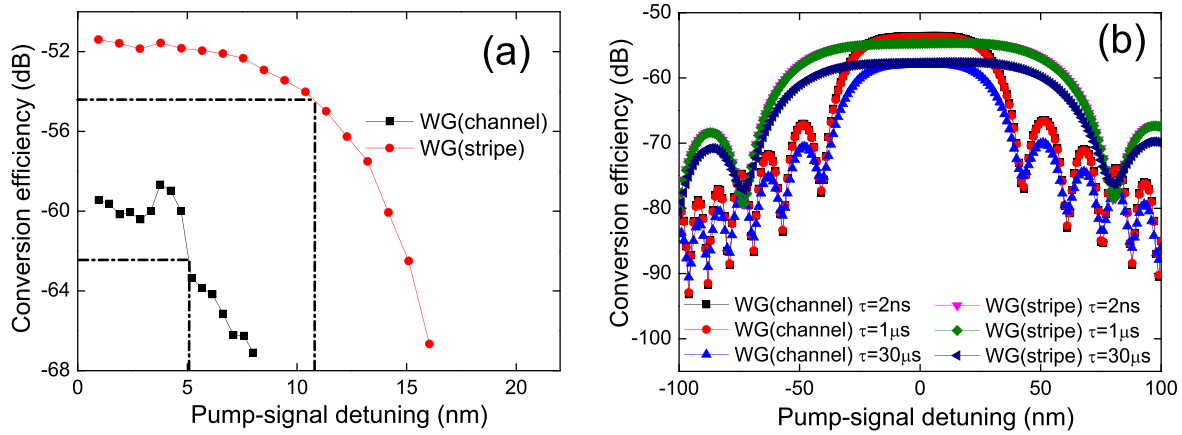

Figure 6. Signal to idler conversion efficiency as a function of the pump-signal detuning for both waveguides used in this study. (a) and (b) Represent experimental and simulated data. In (a), squares and disks are experimental data for the WG(channel) and WG(stripe) waveguides, respectively. Dotted lines refer to the 3 dB data point used to estimate the bandwidth.

WG(channel) and WG(stripe), respectively. These nonlinear coefficient values are much smaller than the one of integrated organic-SOI compound waveguides which have a cladding and slot nonlinearities of 108,000 and 100,000 W^{-1} km^{-1}, respectively [33]. They are also smaller than the highest value of 307,000 W^{-1} km^{-1} for silicon, which is obtained by a tight optical confinement in Si nanowires [33].

Nonlinear absorption could limit the nonlinear processes. This can be quantified by the characteristic figure of merit $FOM = n_2/\lambda\beta$ which is calculated to be 0.007 ± 0.003 and 0.014 ± 0.008 for WG(stripe) and WG(channel), respectively. As reported earlier by Vallaitis *et al* [33], Si shows a FOM of 0.38 ± 0.17, while the FOM values for cladding and slot nonlinearities of integrated organic-SOI system are 1.21 ± 0.19 and 2.19 ± 0.25, respectively. The low FOM in our case shows that, despite the high nonlinearity, the TPA limits the application of Si NC and, therefore, Si NC waveguide could be suitable for long wavelength operations only since in this wavelength range TPA is not effective. Figure 6(a) presents the measured conversion efficiency (η) bandwidth of the Si NC waveguides. η is defined as the ratio of the output idler power to the signal power

$$\eta = 10\log_{10}[P_c(z = L)/P_s(z = 0)] \quad (9)$$

where L is the waveguide length. To measure the conversion efficiency bandwidth, we kept the pump wavelength fixed at 1550 nm and tuned the signal wavelength in an interval which is limited by the EDFA gain region. Using an input pump power of 43.8 mW, the conversion efficiency for WG(stripe) is found to be −51.4 dB, whereas the efficiency remains below −58 dB for WG(channel). On the other hand, the −3 dB bandwidth for WG(channel) and WG(stripe) is 10.5 and 21.7 nm, respectively. In this case, improper phase matching of the WG(channel) along with the larger excited carrier lifetime is responsible for the lower conversion efficiency and bandwidth. To further investigate the effects of carrier lifetime on the efficiency and bandwidth, we have simulated the conversion bandwidth for different τ values using a pump power of 50 mW and a signal power of 1 mW (figure 6(b)). We varied the lifetime from the one of Si waveguide (2 ns) [30] to 30 μs (experimental value of WG(channel)). We found that the larger is the carrier lifetime, the lower is the signal to idler conversion efficiency. The bandwidth is mostly

unaffected since it depends on the dispersion and length of the waveguide. Surprisingly, the measured conversion bandwidth are narrower than the simulated value (∼100 nm for WG(stripe) and ∼56 nm for WG(channel)). Note that, Trita *et al* [21] have reported a conversion bandwidth of 10 nm in a horizontal slot Si NC waveguide.

6. Conclusion

Our results illustrate that isolated Si NCs possess a nonlinear refractive index more than three orders of magnitude larger than silica, two orders of magnitude larger than silicon nitride [8], and one order of magnitude larger than bulk silicon [30]. This large nonlinearity is limited by two photon absorption. When the effect of the matrix are considered the large Si NC nonlinearity is reduced by a factor which depends significantly on the Si NC concentration in the waveguide. Due to the TPA threshold, a pump wavelength longer than twice the Si NC band gap could mitigate the TPA limitations. This can be achieved either by moving to spectral regions longer than ∼2 μm or by using small Si NCs [9]. Since a critical role in the conversion efficiency is played by the excited carrier lifetime, it would be also helpful a reverse biased p-n junction across the waveguide to collect the TPA generated excited carriers and, thus, reduce ECA. Another way to decrease the excited carrier lifetime is to create surface defects on the Si NC by UV excitation. Finally, this work shows that not only the size but also the Si NC concentration has to be optimized in order to use the large Si NC nonlinearities.

Acknowledgments

This work was financially supported by the ITPAR project funded by the Indian DST and the Italian MAE, and by the SIQURO project funded by Provincia Autonoma di Trento. M G and G P acknowledge the support of the staff of the Microfabrication Laboratory of FBK during sample fabrication.

References

[1] Lockwood D J and Pavesi L 2016 *Silicon Photonics III: Systems and Applications (Topics in Applied Physics)* (Berlin: Springer)
[2] Foster M A, Turner A C, Salem R, Lipson M and Gaeta A L 2007 *Opt. Express* **15** 12949–58
[3] Leuthold J, Koos C and Freude W 2010 *Nat. Photon.* **4** 535–44
[4] Özdal B, Koonath P, Raghunathan V and Jalali B 2004 *Opt. Express* **12** 4094–102
[5] Dinu M, Quochi F and Garcia H 2003 *Appl. Phys. Lett.* **82** 2954–6
[6] Espinola R L, Dadap J I, Osgood R M, McNab S J and Vlasov Y A 2004 *Opt. Express* **12** 3713–8
[7] Fukuda H, Yamada K, Shoji T, Takahashi M, Tsuchizawa T, Watanabe T, ichi Takahashi J and ichi Itabashi S 2005 *Opt. Express* **13** 4629–37
[8] Ikeda K, Saperstein R E, Alic N and Fainman Y 2008 *Opt. Express* **16** 12987–94
[9] Wu C L, Lin Y H, Su S P, Huang B J, Tsai C T, Wang H Y, Chi Y C, Wu C I and Lin G R 2015 *ACS Photonics* **2** 1141–54
[10] Yuan Z, Anopchenko A, Daldosso N, Guider R, Navarro-Urrios D, Pitanti A, Spano R and Pavesi L 2009 *Proc. IEEE* **97** 1250–68
[11] Bisadi Z *et al* 2015 *Phys. Status Solidi (a)* **212** 2659–71
[12] Spano R, Daldosso N, Cazzanelli M, Ferraioli L, Tartara L, Yu J, Degiorgio V, Jordana E, Fedeli J M and Pavesi L 2009 *Opt. Express* **17** 3941–50
[13] Martnez A *et al* 2010 *Nano Lett.* **10** 1506–11
[14] Vijayalakshmi S, Grebel H, Yaglioglu G, Pino R, Dorsinville R and White C W 2000 *J. Appl. Phys.* **88** 6418
[15] Hernández S *et al* 2008 *J. Appl. Phys.* **103** 064309
[16] Prakash G V, Cazzanelli M, Gaburro Z, Pavesi L, Iacona F, Franz G and Priolo F 2002 *J. Appl. Phys.* **91** 4607
[17] Ito M, Imakita K, Fujii M and Hayashi S 2010 *J. Appl. Phys.* **108** 063512
[18] Blasco J, Galn J V, Sanchis P, Martnez J M, Martnez A, Jordana E, Fedeli J M and Mart J 2010 *Opt. Commun.* **283** 435–7
[19] Lu S, Zhao C, Zou Y, Chen S, Chen Y, Li Y, Zhang H, Wen S and Tang D 2013 *Opt. Express* **21** 2072–82
[20] Zhang H, Virally S, Bao Q, Ping L K, Massar S, Godbout N and Kockaert P 2012 *Opt. Lett.* **37** 1856–8
[21] Trita A, Lacava C, Minzioni P, Colonna J P, Gautier P, Fedeli J M and Cristiani I 2011 *Appl. Phys. Lett.* **99** 191105
[22] Manna S, Ramiro-Manzano F, Ghulinyan M, Mancinelli M, Turri F, Pucker G and Pavesi L 2015 *Appl. Phys. Lett.* **106** 071109
[23] Matres J, Lacava C, Ballesteros G C, Minzioni P, Cristiani I, Fédéli J M, Martí J and Oton C J 2012 *Opt. Express* **20** 23838–45
[24] Rukhlenko I D 2014 *J. Opt.* **16** 015207
[25] Rukhlenko I D 2013 *Opt. Express* **21** 2832–46
[26] Yldrm H and Bulutay C 2008 *Opt. Commun.* **281** 4118–20
[27] Zeng X C, Bergman D J, Hui P M and Stroud D 1988 *Phys. Rev.* B **38** 10970–3
[28] Cai W and Shalaev V 2009 *Optical Metamaterials: Fundamentals and Applications* (New York: Springer)
[29] Rukhlenko I D, Premaratne M and Agrawal G P 2012 *Opt. Lett.* **37** 2295–7
[30] Gao S, Li Z, Tien E K, He S and Boyraz O 2010 *J. Lightwave Technol.* **28** 3079–85
[31] Navarro-Urrios D, Pitanti A, Daldosso N, Gourbilleau F, Rizk R, Pucker G and Pavesi L 2008 *Appl. Phys. Lett.* **92** 051101
[32] Jalali B, Boyraz O, Dimitropoulos D and Raghunathan V 2005 *Proc. SPIE* **5730** 41–9
[33] Vallaitis T *et al* 2009 *Opt. Express* **17** 17357–68